Chinese Herbal Medicines 15 (2023) 76–85

Contents lists available at ScienceDirect

Chinese Herbal Medicines

journal homepage: www.elsevier.com/locate/chmed

Original Article

Lung protective effects of dietary malate esters derivatives from *Bletilla striata* against SiO_2 nanoparticles through activation of Nrf2 pathway

Di Zhou, Wenhui Chang, Jiaxin Qi, Gang Chen, Ning Li *

Key Laboratory of Computational Chemistry-Based Natural Antitumor Drug, School of Traditional Chinese Materia Medica, Shenyang Pharmaceutical University, Shenyang 110016, China

ARTICLE INFO

Article history:
Received 30 June 2022
Revised 18 September 2022
Accepted 9 October 2022
Available online 4 November 2022

Keywords:
Bletilla striata (Thunb.) Reichb. f.
dietary malate esters derivatives
lung cancer chemoprevention
militarine
SiO_2 nanoparticles-induced A549 cell

ABSTRACT

Objective: To study the protective activities of the dietary malate esters derivatives of *Bletilla striata* against SiO_2 nanoparticles-induced A549 cell lines and its mechanism action.
Methods: The components were isolated and elucidated by spectroscopic methods such as 1D NMR and 2D NMR. And MTT assays was used to tested these components on the A549 cell survival rates and ROS or proteins levels were detected by Western blotting.
Results: A new glucosyloxybenzyl 2-isobutylmalate (a malate ester derivative), along with 31 known compounds were isolated and identified from *n*-BuOH extract of EtOH extract of *B. striata*. Among them, compounds **3**, **4**, **11**, **12** and **13** possessed noteworthy proliferative effects for damaged cells, with ED_{50} of 14.0, 13.1, 3.7, 11.6 and 11.5 μmol/L, respectively, compared to positive control resveratrol (ED_{50}, 14.7 μmol/L). Militarine (**8**) prominently inhibited the intracellular ROS level, and increased the expression of Nrf2 and its downstream genes (*HO-1* and *γ-GCSc*). Furthermore, Nrf2 activation mediates the interventional effects of compound **8** against SiO_2 nanoparticles (nm SiO_2)-induced lung injury. Moreover, treatment with compound **8** significantly reduced lung inflammation and oxidative stress in nm SiO_2-instilled mice. Molecular docking experiment suggested that **8** bound stably to the HO-1 protein by hydrogen bond interactions.
Conclusion: The dietary malate esters derivatives of *B. striata* could significantly increase the viability of nm SiO_2-induced A549 cells and decrease the finer particles-induced cell damages. Militarine is especially promising compound for chemoprevention of lung cancer induced by nm SiO_2 through activation of Nrf2 pathway.

1. Introduction

The finer particles have a seriously impact on the human healthy, as the major sources of ambient air pollutants, especially for lung whose epithelial cells interact with environmental finer particles directly. Many workers were exposed to particles in the long-term, including mining, pottery industries, resulting in lung inflammatory, even lung cancer (Yao et al., 2018). At present, silica nanoparticles have been used as inductive reagent in many experimental researches, which can lead to lung fibrosis or lung cancer because of dysfunction of lung (Bai et al., 2018; Cao et al., 2014; Ouyang et al., 2018). Human lung cancer lines, such as A549 cells, were generally regarded as the receptor of SiO_2 nanoparticles (nm SiO_2) to evaluate the cytotoxicities of finer particulate matters. And accumulating researches suggested that nm SiO_2-induced A549 cells damage may be related to oxidative stress during the past decades (Bolhassani, 2015). Thus, it is imperative need to screen more cytoprotective agents from food supplements to repair the cells damage or increase the cell survival rates and explore how the tonic herbals or food supplements could improve lung cells damage.

Bletilla striata (Thunb.) Reichb. f. (Baiji in Chinese), as a traditional Chinese herbal and edible herb, which was recorded in *Sheng Nong's Herbal Classic* 2000 years ago (Song et al., 2017). *B. striata* was mainly applied in astringent hemostasis, detumescence and myogenesis, and these traditional applications were closely related their anti-inflammatory and anti-oxidative activities. Bibenzyl, dihydrophenanthrene, and diphenanthrene compounds contained in this plant are known to have various biological activities in wound healing in addition to their antioxidant activities (Wei and Hui, 2015; He et al., 2017; Bae et al., 2016).

Researches on 2-isobutylmalates (dietary malate esters derivatives) are increasingly active due to their protective effects in many

* Corresponding author.
E-mail address: liningsypharm@163.com (N. Li).

https://doi.org/10.1016/j.chmed.2022.11.001
1674-6384/

disease models. 2-Isobutylmalates inhibit the activity of monoamine oxidase (MAO), enhance the activity of SOD, promote intelligence, and delay aging in the aging mouse model induced by D-galactose and $NaNO_2$ (Zhang et al., 2006). Furthermore, 2-isobutylmalates can improve the activity of cytochrome *C* oxidase in HaCaT cells, showing a potential to be developed into anti-aging agents. For example, militarine exerts anti-inflammatory activity by inhibiting the release of NO in LPS-induced RAW264.7 cells (Zhao et al., 2018). Despite these advances, the underlying mechanism regarding the lung cancer chemopreventive activity of militarine remains poorly understood. Thus, SiO_2 nanoparticles (nm SiO_2), one of the most important contents of inhalable particles, were applied in this study to induce lung injury to assess the chemo-preventive effect of militarine on lung injury in A549 cells.

2. Material and methods

2.1. Reagents

NMR spectra were recorded on Bruker ARX-400 and 600 M AVIII spectrometers (Berlin, Germany), using TMS as an internal standard. Silica gel (200–300 mesh) for chromatography was produced by Qingdao Ocean Chemical Group (Qingdao, China). Optical rotations were measured using MCP 200 polarimeter from Anton Paar GmbH (Graz, Austria). ODS (50 μm) for column chromatography was afforded by YMC Co., Ltd. (Tokyo, Japan). HPLC separations were performed on a YMC-pack Prep-ODS-A column (250 mm × 20 mm, 5 μm) equipped with a Shimadzu RID-20A UV detector and a Shimadzu LC-6AD series pumping system (Tokyo, Japan). Dimethyl sulfoxide (DMSO), 3-(4,5-dimethylthiazol-2-yl)-2,5-diphenyltetrazolium bromide (MTT), $CDCl_3$, DMSO d_6 and CD_3OD were obtained from Sigma-Aldrich Company (St. Louis, MO, USA). All the chromatographic and analytical grade reagents were obtained from Tianjin DaMao Chemical Company (Tianjin, China). ML385 was purchased from Sellek (Houston, USA).

2.2. Plant materials

The plant material (*Bletilla striata* (Thunb.) Reichb. f.) was supplied by the Shaanxi Tasly Plant Medicine Co., Ltd. (Tianjin, China) in November 2016. Professor Yingni Pan, from School of Traditional Chinese Materia Medica, Shenyang Pharmaceutical University, identified the plant material to be tubers of *B. striata*. A voucher specimen (No. 20161123) was deposited in School of Traditional Chinese Materia Medica of Shenyang Pharmaceutical University.

2.3. Extraction and isolation

The dried and powdered tubers of *B. striata* (16 kg) were refluxed with 95% EtOH (three times, 3 h for each). The extract was evaporated to dryness under vacuum to afford a crude residue (EB, 1.82 kg, 11.38%), which was partitioned successively with petroleum ether (PE), ethyl acetate (EtOAc) and *n*-BuOH. *n*-BuOH extract (BEB, 300.0 g) was subjected to column chromatography over silica gel and eluted with CH_2Cl_2 and MeOH mixtures in a step gradient manner to afford eight fractions (Fr.1–8). Fr.1 was fractionated further on a ODS column using gradient elution of MeOH-H_2O (0:100–100:0) to give 30% part and 50% part. Subfractions were in turn partitioned with HPLC to get compounds **31** (17.0 mg), **32** (15.6 mg), **4** (31.3 mg), **5** (15.1 mg), **6** (57.1 mg), and **11** (15.2 mg). Separation of Fr. 2 and 3 were performed by ODS chromatography and further separated by HPLC to give compounds **12** (32.0 mg), **13** (12.3 mg), **21** (12.3 mg), **24** (13.6 mg), **26** (22.3 mg), **28** (62.2 mg), **29** (21.0 mg). And Fr. 4 was loaded on a ODS column (75 cm × 3.5 cm, 50 μm), eluting with MeOH and further purified by HPLC with ODS column (250 mm × 10 mm, 50 μm) to yield compounds **17** (18.4 mg), **18** (21.3 mg), **20** (21.6 mg), **22** (17.2 mg) using MeOH/H_2O (64: 36) as eluting solvent. Fr. 6 was subjected to ODS column (MeOH-H_2O, 0:100–100:0) and similar fractions were pooled together followed by TLC analysis. Among them, 30% part was chromatographed over HPLC and eluted with MeOH-H_2O (55: 45) to yield compounds **2** (20.2 mg), **5** (73.2 mg), **13** (120.2 mg) and **23** (16.6 mg). Using the same method, 45% part and 55% part were separated by HPLC to obtain compounds **24** (22.8 mg) and **25** (37.7 mg), **27** (17.4 mg), **28** (45.9 mg), **29** (25.2 mg) and **30** (17.0 mg), respectively. Compounds **1** (15.6 mg), **2** (64.2 mg), **3** (24.8 mg), **7** (19.9 mg) were obtained from Fr. 7 by purification on HPLC with MeOH/H_2O (53: 47) and MeOH/H_2O (60: 40) as the eluent, respectively. Equally, Fr. 8 was firstly fractioned by ODS column (100 cm × 3.5 cm, 50 μm) and yield 30% part and 55% part. Compounds **8** (66.7 mg), **9** (41.2 mg), **10** (12.0 mg), **14** (10.2 mg), **15** (48.0 mg) were purified from 30% part. Then 55% part was purified by HPLC with ODS column (250 mm × 10 mm, 50 μm) using MeOH/H_2O (55:45) as a mobile phase, and provided compound **16** (43.8 mg), compound **19** (27.2 mg).

2.4. Acid hydrolysis of compound 1 and HPLC analysis for sugar residues

Compound **1** (1.0 mg) was heated in 4 mol/L HCl (2 mL) for 3 h in a H_2O bath at 90 °C. After cooling, mixtures were extracted by CH_2Cl_2 and get CH_2Cl_2 extract. Then aqueous layer was evaporated to dryness. The water layer and D-glucose (authentic sample, 1.0 mg) were added in 3.0 mg L-cysteine methyl ester and were dissolved in pyridine (1 mL) and heated at 60 °C for 1 h and then *O*-tolyl isothiocyanate (5 μL) was added to the mixture and heated further for 1 h. The reaction mixture was analyzed by HPLC and detected at 250 nm. The HPLC analysis was carried out on a Shimadzu SPD-20A (UV/Visible Detector, Shimadzu, Tokyo, Japan) using a Shimpack ODS (H) KIT (5 μm particle size, 4.6 mm × 250 mm) at 35 °C with a flow rate of 1 mL/min. Mobile phase was a mixture of 0.1% formic acid–water (A: 75%) and acetonitrile (B: 25%) (He et al., 2017).

2.5. Cell cultures

Human non-small lung cancer cells A549 were cultured at 1640 medium with 10% FBS for 37 °C (5% content of CO_2). Before treated with drugs, 50 nm silica particles are weighed for appropriate amount and put into 5 mL EP tube. They were irradiated overnight by ultraviolet lamp to sterilize. Using fresh serum-free medium, 2 mg/mL reserve solution was prepared, whirled for 30 s and ultrasound for 30 min. Then, reserve solution was diluted to working fluid concentration by fresh serum-free medium.

2.6. MTT assays for cytotoxicities of SiO_2-induced A549 cells

Cells were plated in 96-well plates at a density of 10^5 cells/well. After cells were cultivated for 24 h with cells adhered to the wall, the supernatant was discarded. The cells were further cultured for 24 h by adding a suspension of 20 μg/cm^2 nm SiO_2. The cells were treated with extracts or compounds for 24 h at concentrations of 100 μg/mL, 50 μg/mL, 10 μg/mL, and 1 μg/mL for extracts, 100 μmol/L, 50 μmol/L, 10 μmol/L, and 1 μmol/L for compounds, respectively. After 24 h, the cell counting was determined by MTT method. Absorbance of each well was measured at 490 nm with automatic enzyme marker. ED_{50} was determined as the concentration of each compound which induced 50% inhibition of cell growth. The values represent averages of three independent experiments. Resveratrol was used as a positive control reagent.

2.7. Intracellular ROS measurement for SiO_2-induced A549 cells

Intracellular ROS productions were performed using 2′,7′-dichl orodihydrofluorescein diacetate (DCFH-DA, Nanjing Jiancheng, 100 T–500 T) according to the protocols. Cells were cultured with 1640 culture medium containing 10% FBS at a density of 2.5×10^4 cells/well at 37 °C (5% content of CO_2). After 24 h, cells were treated 20 μg/cm^2 nm SiO_2 with 20 μmol/L concentration of compounds. And cells were further incubated with 1 μL (DCFH-DA) for 30 min at room temperature. The cells were washed with PBS and the cell fluorescence intensities of cells were read using a flow cytometry (BD FACSAria II) from each well. ROS production was determined by flow cytometer and observed by fluorescence microscope.

2.8. Flow cytometry analysis of apoptosis

The rate of apoptosis stimulated by drugs was measured using Annexin V-FITC apoptosis detection kit (Beyotime, Haimen, China). A549 cells were planted into 60 mm petri dishes, pretreated with militarine (25 μmol/L) for 2 h, then treated with nm SiO_2 (20 μg/cm^2) and militarine for 24 h. After the pretreatment with militarine (**8**) for 2 h, it was co-cultured with nm SiO_2 for 24 h. Then the cells were collected and washed with PBS (centrifuged at 1800 rpm for 5 min). After re-suspending with binding buffer, the cells were incubated with 5 μL of Annexin V FITC for 15 min followed by 5 μL of propidium iodide. Finally, the samples were detected by Flow Cytometer (BD Biosciences, New Jersey, USA) and quantified with Flow Jo 7.6.

2.9. Hoechst 33258 staining

Hoechst 33258 Staining Kit (Beyotime, Haimen, China) was used to evaluate morphological changes of apoptotic A549 cells. A549 cells were planted into 24-well plates overnight and pretreated with militarine (25 μmol/L) for 2 h, then treated with nm SiO_2 (20 μg/cm^2) and militarine for 24 h. After the fixation with 4% paraformaldehyde for 10 min, the cells were washed with PBS twice and stained with Hoechst 33258 for 5 min in dark conditions. Finally, cellular morphology was observed by fluorescence microscope (Olympus, Tokyo, Japan).

2.10. Immunofluorescence

A549 cells were planted into 24-well plates overnight and were treated as described above, and then fixed with 4% paraformaldehyde for 30 min. Afterward, the cells were washed with PBS for three times, and incubated with 5% bovine serum albumin for 1 h. Subsequently, the cells were incubated with Nrf2 antibody (1: 200) overnight at 4 °C. After washing three times in TBST, the cells were stained with a fluorescent goat anti-rabbit secondary fluorescent antibody (1:200, Protein Tech, New York, USA) in the dark for 1 h. Finally, the cells were incubated with DAPI for 3 min. Fluorescence images were detected by upright fluorescence microscope (Berlin, Germany).

2.11. Western blotting assays

The mouse lung tissues were flushed with PBS to remove blood. Subsequently, RIPA (radio immunoprecipitation assay) was added, and the tissues were homogenized by using the homogenizer. The samples were placed on ice for 30 min and centrifuged at 4 °C at 15,000 r/min for 15 min. The supernatant was taken for subsequent experiments. The equal amounts of protein samples were quantitated by BCA (bicinchoninic acid). Then the samples were loaded and separated by SDS-polyacrylamide gel (Beyotime, Haimen, China) and transferred on PVDF membranes. The PVDF membranes were blocked with skim milk for 1 h and incubated overnight at 4 °C with the primary antibodies against β-actin (1:1000 dilution, CST, Boston, USA), Nrf2, Bcl-2, Bax, (1:1000 dilution, Abcam, Cambridge, UK), HO-1, γ-GCSc (1:500 dilution, Santa Cruz, CA, USA). After blocking, the PVDF membranes were washed three times in TBST and then incubated with secondary antibodies (WanLei, Shanghai, China) for 1.5 h. Finally, the blots were washed three times in TBST and the protein bands were visualized by using ECL (Bio-rad, New York, USA). The intensity of protein bands were quantitated with ImageJ software.

2.12. Molecular docking study

Molecular docking study was carried out using Glide. The crystal structure of HO-1 in complex with SLV-8289 (PDB: 6EHA) was used referring to the publicized text (Mucha et al., 2019).

2.13. Statistical analysis

All values in the figures and table are expressed as mean ± Standard Error of Mean (SEM). The statistical significance of any difference in each parameter among the groups was evaluated by one-way analysis of variance (ANOVA) followed by Tukey's test using Prism 6.0 software, and $P < 0.05$ was considered statistically significant.

3. Results

3.1. Activity screening of EB and BEB

The A549 cells damages models induced by nm SiO_2 were applied to evaluate the cytoprotection of the EtOH extract (EB) and BEB of *B. striata*. These extracts displayed potent protective activities for A549 cells, with ED_{50} values of 10.3, 17.3 μg/mL, respectively. And BEB was the effective fractions of the plant. We further studied the lung protective effects of BEB *in vitro*.

3.2. Structural identification

To further determine the effective material basis of BEB, phytochemical isolations of *n*-BuOH extract of the ethanol extract of the tubers of *B. striata* afforded 32 compounds (Fig. 1) by means of chromatographic methods and recrystallization, including one new glucosyloxybenzyl 2-isobutylmalate, seven known glucosyloxybenzyl 2-isobutylmalates and other compounds. Finally, their structures were determined as follow: (*Z*)-2-(2-methylpropyl) butenedioic acid-4-β-D-glucopyranosyloxybenzyl ester (**1**), gymnoside I (**2**) (Yue et al., 2010), gymnoside II (**3**) (Yue et al., 2010), 1-(4-*O*-glucopyranosyloxybenzyl) 4-methyl (2*R*)-2-isobutylmalate (**4**) (Huang et al., 2002), (*Z*)-2-(2-methylpropyl) butenedioic acid bis(4-β-D-glucopyranosyloxybenzyl) ester (**5**) (Huang et al., 2002), dactylorhin A (**6**) (Huang et al., 2002), gymnoside III (**7**) (Yue et al., 2010), militarine (**8**) (Yue et al., 2010), tortoside A (**9**) (Cai et al., 2004), 4-allyl-2, 6-dimethoxyphenol glucoside (**10**) (Guan et al., 2009), bletilloside A (**11**) (Zhao et al., 2018), shancigusin I (**12**) (Morikawa et al., 2006), bleformin J (**13**) (Lin et al., 2016), 4-hydroxy-*trans*-cinnamomic acid 4-β-D-glucopyranosyloxybenzyl ester (**14**) (Zidorn et al., 2001), *trans*-*p*-hydroxycinnamic acid (**15**) (Miao et al., 2008), *p*-hydroxybenzaldehyde (**16**) (Ying et al., 2009), 4-methoxybenzyl alcohol (**17**) (Xiang et al., 2017), *p*-hydroxyphenylacetic acid methyl ester (**18**) (Feng et al., 2009), 4-methoxy catechol (**19**) (Zhou et al., 2010), *p*-methoxyphenylpropionic acid (**20**) (Pcolinski et al., 1995), *p*-hydroxybenzoic acid (**21**) (Gouvêa et al., 2016), vanillin (**22**) (Duan et al., 2013), 4-

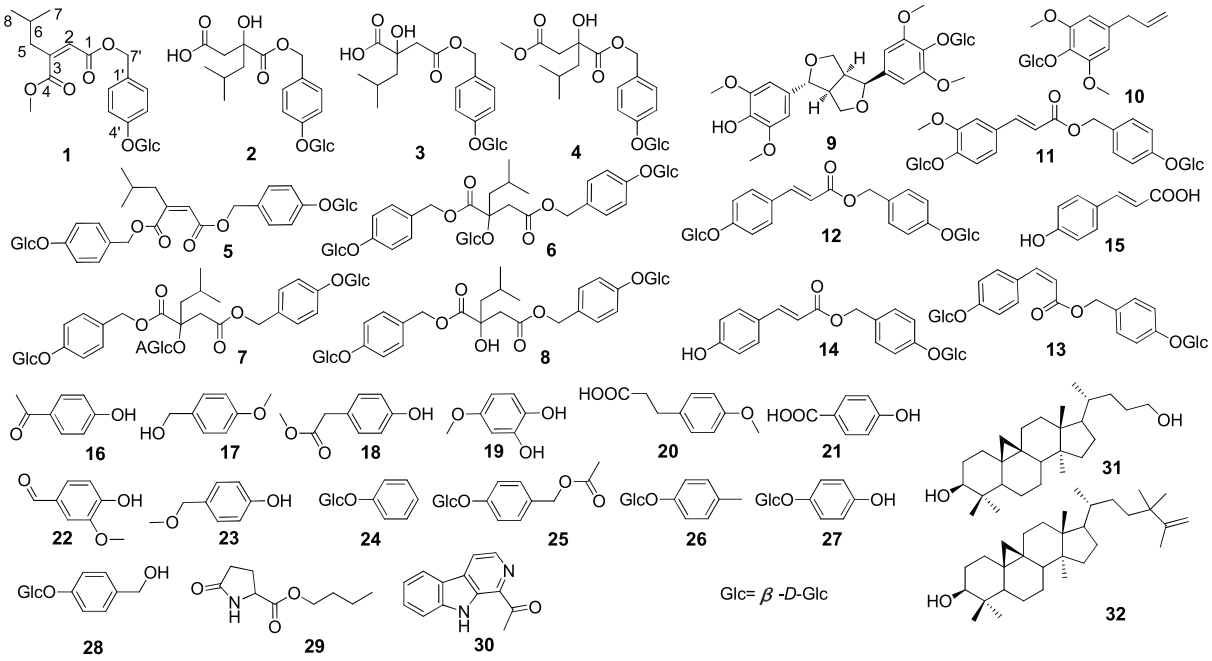

Fig. 1. Structures of compounds **1**–**32**.

(methoxymethyl)phenol (**23**) (Wang et al., 2012), phenyl-*β*-*D*-glucopyranoside (**24**) (Chen et al., 2008), 4-[(acetyloxy)methyl] phenyl-*β*-*D*-glucopyranoside (**25**) (Li et al., 2006), *p*-methylphenyl-1-*O*-*β*-*D*-glucopyranoside (**26**) (Duan et al., 2013), arbutin (**27**) (Jiang et al., 2017), gastrodin (**28**) (Han et al., 2015), *n*-butyl pyroglutamate (**29**) (Tang et al., 2001), 1-acetyl-*β*-carboline (**30**) (Tang et al., 2001), cycloneolitsol (**31**) (Tang et al., 2001), (3α, 5α)-4,4,14-trimethyl-9,19-cyclocholane-3,24-diol (**32**) (Tang et al., 2001).

Compound **1**, a colorless oil, had a molecular formula of $C_{22}H_{30}O_{10}$ based on ^{13}C NMR data and on a quasi-molecular ion peak at *m*/*z* 477.1041 $[M+Na]^+$ (calcd. 477.1043 for $C_{22}H_{30}NaO_{10}$) in HRESI-MS that required 15 indices of hydrogen deficiency. The ^1H NMR spectrum of **1** showed two methyls at 0.85 (6H, d, *J* = 6.6 Hz, Me-7, 8), two methylenes at 2.21 (2H, dd, *J* = 7.2, 1.0 Hz, H-5) and 5.12 (2H, s, H-7′), a methine at 1.68 (1H, m, H-6), a methoxyl at 3.59 (3H, s, OCH_3) and an AA'BB'-type aromatic pattern [7.31 (2H, d, *J* = 8.4 Hz, H-2′, 6′), 7.03 (2H, d, *J* = 8.4 Hz, H-3′, 5′)], a glucopyranosyl moiety at 4.87 (1H, d, *J* = 7.2 Hz, H-1″), together with an olefinic proton at 6.02 (1H, s, H-2). Compared with known compound 1-(4-*O*-glucopyranosyloxybenzyl)-4-methyl (2*R*)-2-isobutylmalate, the spectral data showed great similarity, an obvious difference could be observed in that the double bond between C-2 and C-3 positioned in **1** replaced the single bond in known compound, showing 121.0 (C-2), 148.6 (C-3) in ^{13}C NMR. It was further confirmed by HMBC correlations from H-3 to C-1, C-4 and from H-5 to C-3. In addition, the *Z*-configuration of the double bond in **1** was clarified by comparing the chemical shift of olefinic proton (H-2, 6.02) with those previously reported. According to the reported data, the olefinic proton signal in *E*-configuration (δ_H 6.49–7.08) often exists in a lower field than that in the *Z*-configuration (δ_H 5.48–6.22) in DMSO.[11, 33]HMBC spectrum also established unequivocally that the glucose moiety was connected to the benzyl moiety at C-4′. Acid hydrolysis of **1** produced glucose as the sole sugar identified on the basis of derivatization by comparing with an authentic sugar sample. Thus, the structure of **1** was determined as (*Z*)-2-(2-methylpropyl) butenedioic acid-4-*β*-*D*-glucopyranosyloxybenzyl ester, as shown in Fig. 2. The ^1H and ^{13}C NMR data, see Table 1.

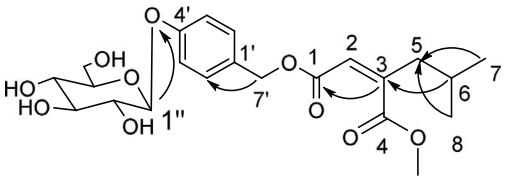

Fig. 2. Key HMBC (⟶) correlations of compound **1**.

3.3. Protective effects of isolates on nm SiO_2-induced A549 cells damages

To figure out the effective constituents of the *n*-BuOH extract of EB of *B. striata*, lung protective effects of the 32 purified components were further assayed. The results indicated that compounds **4**, **11**, **12**, and **13** possessed significant protective effects with ED_{50} values of 13.1, 3.7, 11.6 and 11.5 μmol/L, compared with the positive control, resveratrol (14.7 μmol/L) (Table 2, Fig. 3). In addition, compounds **3**, **8**, **23**, **24**, **25**, and **26** revealed moderate proliferative activities at a concentration-dependent manner, ED_{50} ranging from 16.0 to 29.6 μmol/L. Compounds **14**, **27**, and **28** manifested weak protective function at 100 μmol/L.

According to the above-mentioned results, relationships between structures and activities were concluded as follows. Firstly, for glucosyloxybenzyl 2-isobutylmalate, esterification of 4-carboxyl was detrimental to the protective effects, such as compounds **2** *vs* **4**. Secondly, comparing compounds **11** and **12**, the presence of 4-OCH_3 was beneficial to activity for cinnamates. Similarity, glycosylation of 4-OH contributed to the activity, such as compounds **12** *vs* **14**. Therefore, glucosyloxybenzyl 2-isobutylmalates and cinnamates were the main material basis of EBE of the tubers of *B. striata* to protect the damaged cells.

3.4. Measurement of ROS production on nm SiO_2-induced A549 cells damages

In order to assess whether isolates induces ROS production, the nm SiO_2-induced A549 damage cells were exposed to compounds

Table 1
^{1}H (600 MHz) and ^{13}C (150 MHz) spectra data of compound **1** in DMSO d_6.

No.	δ_H, J (Hz)	δ_C	No.	δ_H, J (Hz)	δ_C
1		167.9	4′		157.4
2	6.02, s	121.0	5′	7.03, d, 8.4	116.1
3		148.6	6′	7.31, d, 8.4	129.9
4		164.9	7′	5.12, s	66.3
5	2.21, dd, 7.2, 1.0	42.7	1″	4.87, d, 7.2	100.2
6	1.68, m	26.0	2″	3.23, m	73.2
7	0.85, d, 6.6	21.9	3″	3.26, m	76.6
8	0.85, d, 6.6	21.9	4″	3.15, t, 7.2	69.7
1′		128.7	5″	3.22, m	77.0
2′	7.31, d, 8.4	129.9	6″	3.68, m; 3.45, m	60.7
3′	7.03, d, 8.4	116.1	OCH_3	3.59, s	51.7

Table 2
Protective effects of extracts and isolated compounds from *B. striata* on damages of nm SiO_2-induced A549 cells (mean ± SEM).[d]

Sample names	ED_{50}[a]	Sample names	ED_{50}[a]
EB[b]	10.3 ± 2.5	**13**	11.5 ± 2.7
BEB[b]	17.3 ± 1.7	**23**	29.6 ± 1.3
3	14.0 ± 1.9	**24**	20.3 ± 5.2
4	13.1 ± 0.8	**25**	25.3 ± 1.6
8	19.5 ± 3.1	**26**	26.1 ± 0.9
11	3.7 ± 1.7	resveratrol[c]	14.7 ± 1.8
12	11.6 ± 3.3		

Note: [a] ED_{50} (μg/mL for extracts and μmol/L for compounds). [b] EB: total ethanol extract of *B. striata*; BEB: *n*-BuOH extract of ethanol extract of *B. striata*. [c] Resveratrol was used as a positive control. [d] Compounds **1**, **2**, **5**, **6**, **7**, **9**, **10**, **15**, **16**, **17**, **18**, **19**, **20**, **21**, **22**, **29**, **30**, **31** and **32** showed no protective activity at tested concentrations (1, 10, 30, 100 μmol/L); Compounds **14**, **27** and **28** showed weak protective activities at 100 μmol/L.

with a concentration of 20 μmol/L, after which fluorescent probes DCFH-DA was applied to measure the levels of intracellular ROS. Compounds **3**, **4**, **8**, **11**, **12**, **13**, **23**–**26** were performed to ROS assays due to the preliminary screening results and non-cytotoxicities. Treatment of A549 cells with SiO_2-nanoparticles rapidly increased intracellular ROS level, which was effectively attenuated by pre-treatment with isolates. The outcomes suggested that ROS production was decreased by compounds **4**, **8**-treated, compared to positive control (resveratrol), as shown in Fig. 4. In addition, compounds **3**, **11**, **12**, **13**, **23**, and **25** could inhibit the production of ROS, compared to the SiO_2-induced groups. These results suggested that isolates may protect cells injury by the reduction of ROS generation.

3.5. Effect of militarine on nm SiO_2-induced cytotoxicity in A549 cells

The results showed that militarine was toxic free (1–50 μmol/L) and was able to reverse the nm SiO_2-induced decrease in cell viability (Fig. 5A). Moreover, the morphological changes of decreased cell density and floating dead cells were observed after nm SiO_2 treatment (20 μg/cm^2). Notably, the co-treatment of nm SiO_2 and militarine rescued the damage caused by nm SiO_2 in A549 cells (Fig. 5B).

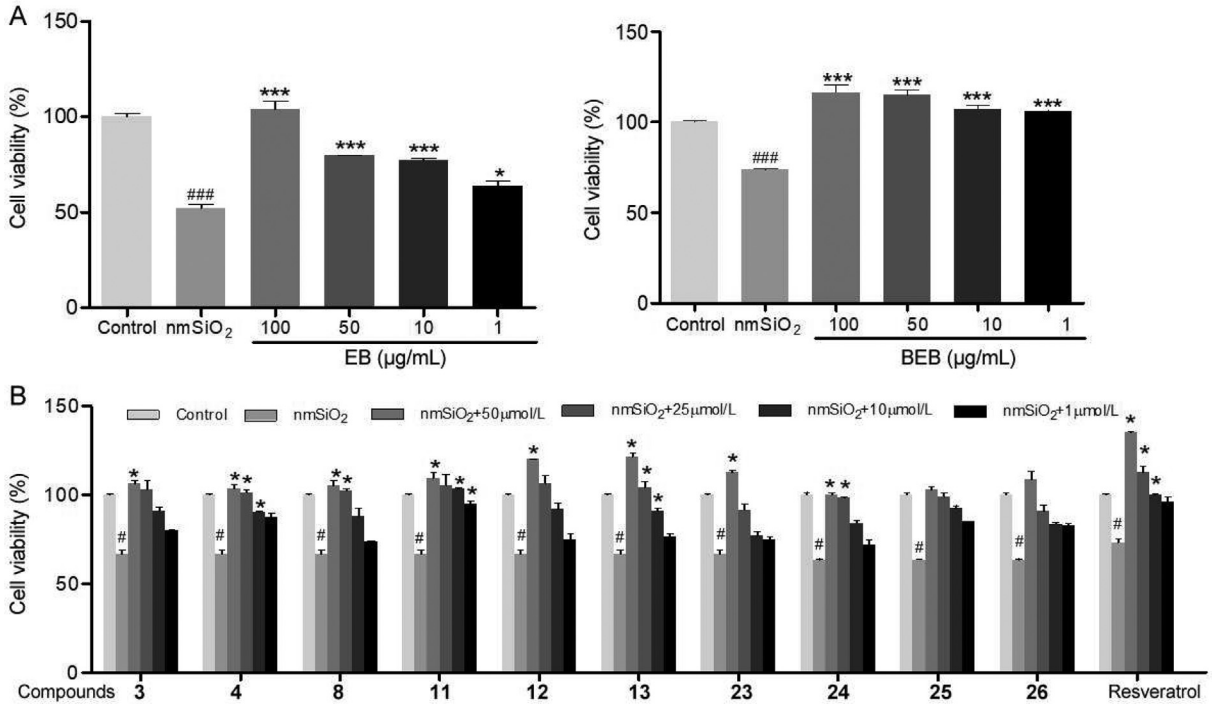

Fig. 3. Protective effects of ethanol extract (EB), *n*-BuOH extract (BEB) and isolated compounds of *B. striata* on damages of nm SiO_2-induced A549 cells. Protective effects of EB and BEB (A), Protective effects of compounds **3**, **4**, **8**, **11**, **12**, **13**, **23**, **24**, **25**, **26** and resveratrol (B). (Each bar represents the means ± SEM of three independent experiments. Significance: $^{*}P < 0.05$, $^{***}P < 0.001$ *vs* nm SiO_2 groups; $^{\#}P < 0.05$, $^{\#\#\#}P < 0.001$ *vs* control group).

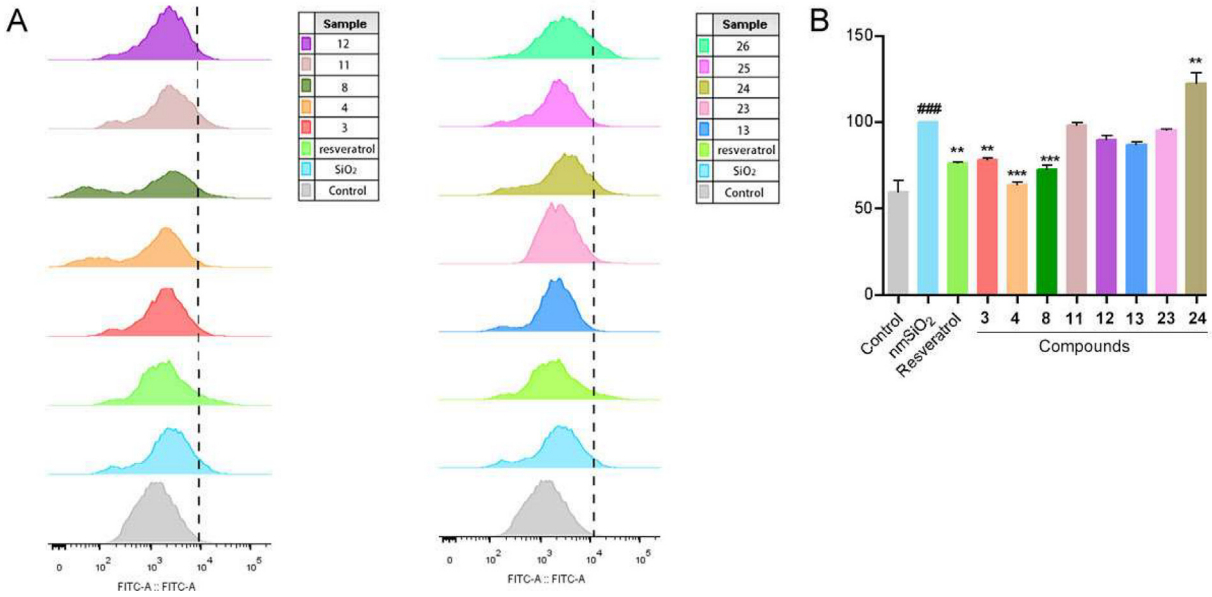

Fig. 4. Effects of isolates on nm SiO_2-induced ROS production. The fluorescence intensities of cells were measured by a flow cytometry method (A) and Enzymatic marker (B). (Each bar represents the means ± SEM of three independent experiments. Significance: $^{**}P < 0.01$, $^{***}P < 0.001$ *vs* SiO_2 groups; $^{\#\#\#}P < 0.001$ *vs* control group).

3.6. Cell apoptosis detection

Hoechst 33258 staining (Fig. 6A) showed that the nuclei displayed homogeneous staining without the presence of significant changes in the control group. Cytoplasmic staining and nuclear contraction were observed in the nm SiO_2 group. This phenomenon is greatly reversed after the treatment of militarine in A549 cells. Western blot results (Fig. 6B) showed that militarine increased the Bcl-2 level and decreased the Bax level, indicating that militarine was able to inhibit nm SiO_2-induced apoptosis in A549 cells.

3.7. Protective effect of militarine on nm SiO_2-induced oxidative stress

DCFH-DA fluorescent probe was used to evaluate the Intracellular ROS (Fig. 7A), the green fluorescence intensity was significantly enhanced when treated with nm SiO_2 alone, suggesting an elevated ROS level. The ROS-inducing effect of nm SiO_2 was eliminated when co-treated with militarine compared with nm SiO_2 group. Furthermore, a consistent result was obtained with the flow cytometry experiment. When treated with nm SiO_2, the DCF positive rate was increased compared with the control group. Militarine treatment could effectively decrease the nm SiO_2-induced

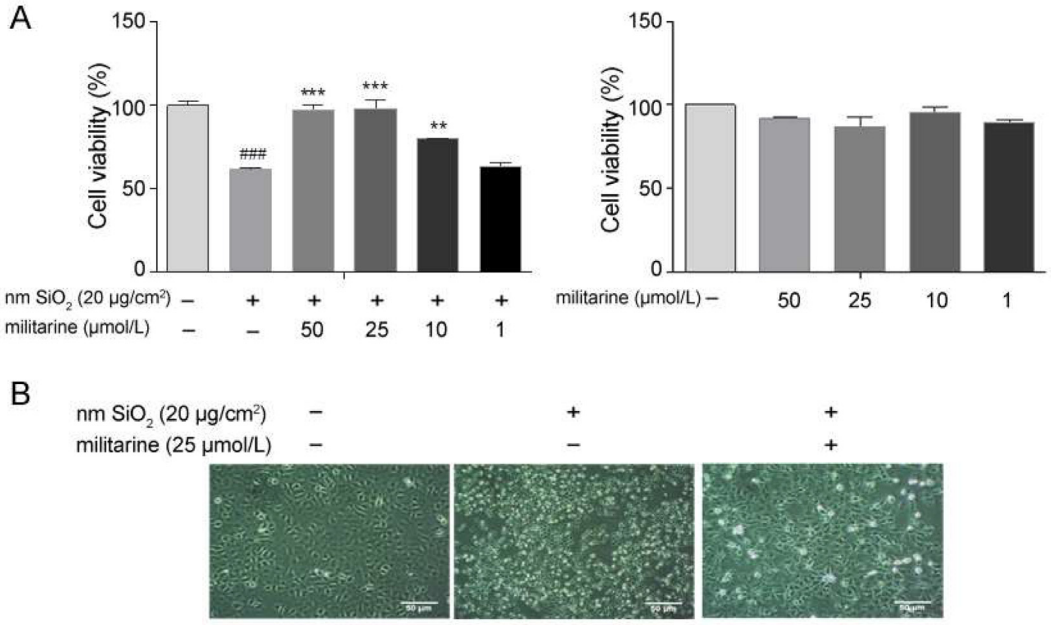

Fig. 5. Effect of militarine on nm SiO_2-induced cytotoxicity in A549 cells. Cell viability of different concentrations of nm SiO_2 and militarine in A549 cells (A), and morphological detection of A549 cells exposed to nm SiO_2 (40×, scale bar = 50 μm) (B). $^{\#\#\#}P < 0.001$ *vs* control group; $^{**}P < 0.01$, $^{***}P < 0.001$ *vs* nm SiO_2 group.

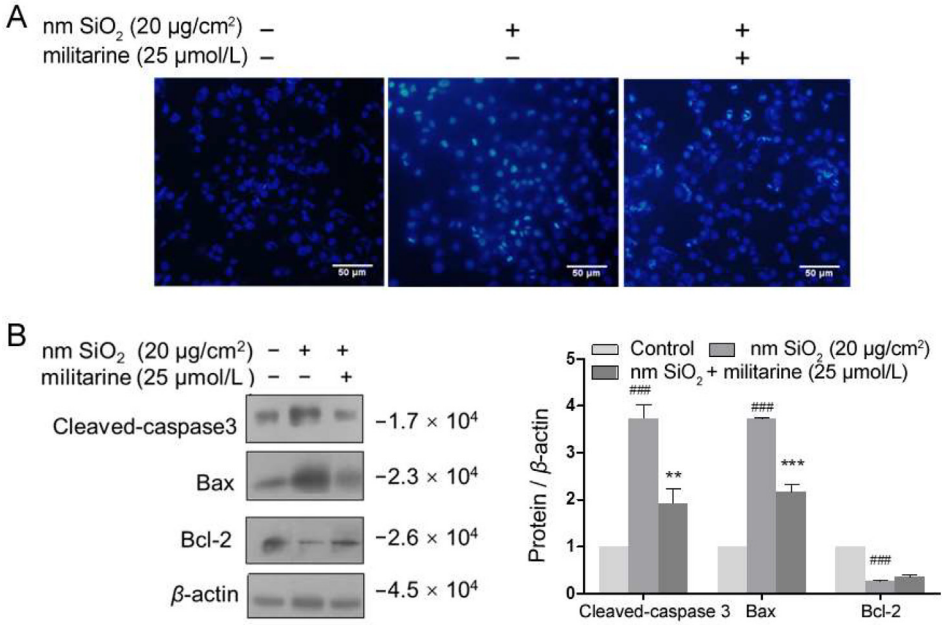

Fig. 6. Effects of militarine on nm SiO_2-induced cell apoptosis. Hoechst 33258 staining by fluorescence microscope (A), Western blots of Pro-caspase 3, Cleaved-caspase 3, Bax and Bcl-2, quantitative results are presented as mean ± SD from three independent experiments (below) (B). $^{###}P < 0.001$ *vs* control group; $^{**}P < 0.01$, $^{***}P < 0.001$ *vs* nm SiO_2 group.

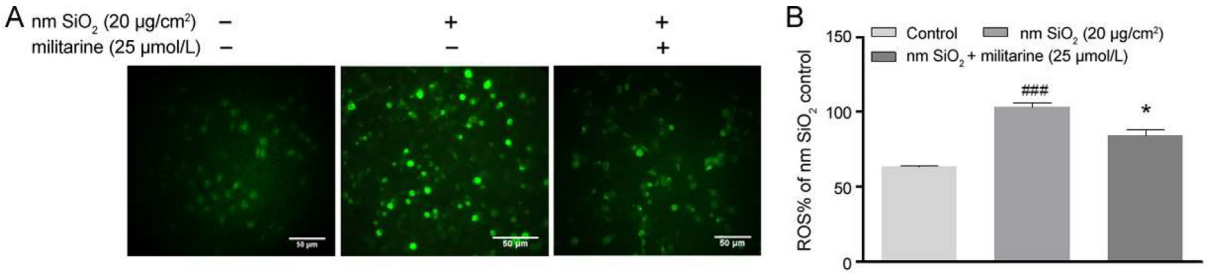

Fig. 7. Effects of militarine on nm SiO_2-induced oxidative stress in A549 cells. Accumulation of ROS using DCFH-DA probe observed by fluorescence microscope (A). Intracellular ROS were measured using DCFH-DA staining by flow cytometry, and quantitative results are presented as mean ± SD from three independent experiments (right) (B). $^{###}P < 0.001$ *vs* control group; $^{*}P < 0.05$ *vs* nm SiO_2 group.

increase of DCF positive rate and restore the intracellular ROS level to a relatively normal level (Fig. 7B). In summary, militarine was effective in preventing nm SiO_2-induced oxidative stress in A549 cells by decreasing oxidative stress.

3.8. Protective effect of militarine is involved in Nrf2 signaling pathway

To further demonstrate whether militarine inhibit nm SiO_2-induced lung injury through Nrf2 signaling pathway, ML385, a specific Nrf2 inhibitor, was adopted in following experiments. The results showed that ML385 could effectively down-regulate the Nrf2 expression compared with the nm SiO_2 group (Fig. 8A). After adding ML385, MTT assay (Fig. 8B) showed that the cell viability of A549 cells was significantly lower than that the co-treatment experiment of nm SiO_2 and militarine, which indicated that co-treated with militarine and ML385 could inhibit the cell viability, and consequently suppressed the lung protection by militarine.

3.9. Effect of militarine on modulation of Nrf2 signaling pathway

To explore whether co-treatment with militarine can affect Nrf2 pathway, the Western blot method was applied to detect the changes of protein levels. The results revealed that nm SiO_2 moderately increased the expression of Nrf2 and its downstream phase II antioxidant enzymes, including HO-1 and γ-GCSc (Fig. 8C). The militarine group significantly further promoted the level of Nrf2 and its downstream proteins compared with nm SiO_2 group. Next, upright fluorescence microscope was applied to track Nrf2 specifically. Compared with control group, the fluorescence intensity was significantly promoted when treated with nm SiO_2 alone, indicating the up-regulated expression of Nrf2. The fluorescence intensity was evidently further enhanced after militarine stimulation in A549 cells (Fig. 8D). These data suggested militarine was effective on the protection against nm SiO_2-induced oxidative stress through the activation of Nrf2.

3.10. Molecular docking

In order to discuss the plausible mode of interaction between HO-1 and the bioactive compound **8**, molecular docking was performed to examine their relative binding energies and possible binding sites with HO-1 (Mucha et al., 2019). The co-crystal of HO-1 with ligand SLV-8289 (PDB: 6EHA) that acts as an inhibitor of HO-1 was used in the docking experiment. By molecule docking, we clearly observed that the bioactive compound **8** could occupy the HO-1 hydrophobic binding groove (Fig. 9), displaying the

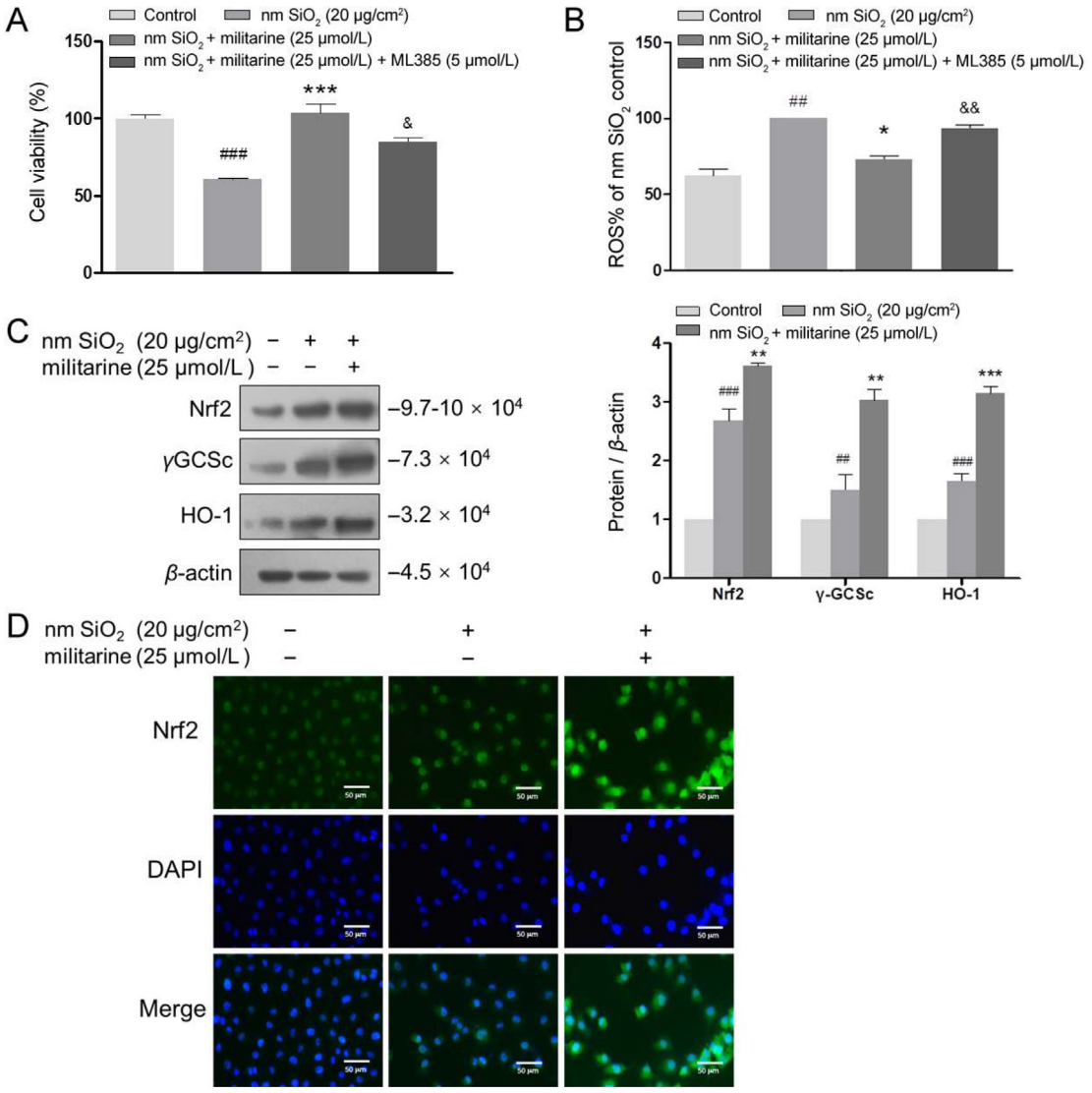

Fig. 8. Militarine (25 μmol/L) actived Nrf2 signaling pathway. Cell viability after treatment with ML385 (A), Intracellular ROS (B). Protein expression of Nrf2 signaling pathway in A549 cells. Representative Western blots of Nrf2, γ-GCSc and HO-1, quantitative results are presented as mean ± SD from three independent experiments (below) (C). Cells were labeled for Nrf2 (green) and nucleus (blue) (D). $^{\#\#}P < 0.01$, $^{\#\#\#}P < 0.001$ *vs* control group; $^{*}P < 0.05$, $^{**}P < 0.01$, $^{***}P < 0.001$ *vs* nm SiO_2 group; $^{\&}P < 0.05$, $^{\&\&}P < 0.01$ *vs* nm SiO_2 + militarine group.

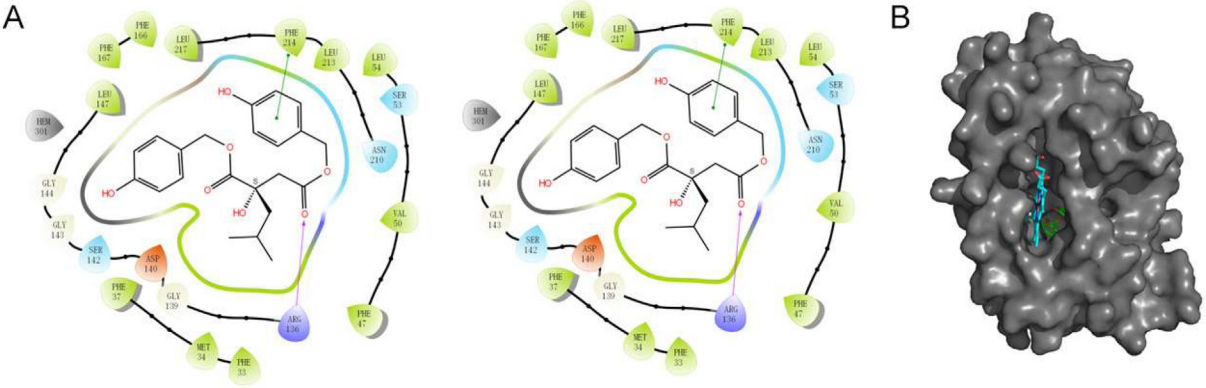

Fig. 9. Predicted hydrogen bond and electrostatic interactions between **8** and HO-1. Hydrogen bond interactions of **8** and HO-1 complex (A), Hydrogen bond interactions of SLV-8289 (PDB: 6EHA) and HO-1 complex (B).

similar binding mode comparing with that of the 6EHA (docking score: −11.31). Among all the interactions between **8** and HO-1, the hydrogen bonds accounted for the total docking score (−12.72) provided by Glide (extra precise mode). Compound **8** could form hydrogen bonds with residues of Asn210 and HEM301 in Fig. 9. To further confirm the stability of the complex of **8** and HO-1, the binding energy was tested with MM-GBSA method. The results showed that the binding energy was −38.24 kcal (ΔG_{Bind} value) for **8**, showing moderate binding affinity compared with that of 6EHA (−44.54 kcal).

4. Discussion

Oxidative stress plays an important role in the pathogenesis of nm SiO_2-induced lung intoxication. SiO_2-induced toxicity has been reported to be related to the change of oxidant/anti-oxidant balance. Oxygen free radicals have been regarded as second messenger. In the present study, we choose specific mediators that are involved in oxidant stress and inflammation in the lung of nm SiO_2-induced mice, that is, HO-1, γ-GCSc proteins, and so on.

Studies *in vitro* and *in vivo* showed that apigenin possesses antioxidant, anti-inflammatory, anti-carcinogenic and neuroprotective properties. In the present study, BEB exhibited significant protective effect on damaged cells *in vitro* and the effective material basis of BEB was explored.

As a result, glucosyloxybenzyl 2-isobutylmalates (named malic acid derivatives, malate esters derivatives or 2-(2-methylpropyl)-butanedioic acid derivatives), as edible natural products, are a class of important active and characteristic compositions in the fruits, food, and medicines, which were mainly distributed in Orchidaceae family, such as, *Gymnadenia conopsea* (L.), *Pleione bulbocodioides* (Franch.) Rolfe, *Grammatophyllum speciosum* Blume, and so on, including the plant *B. striata*. These compositions derived from the major constituents of malic acid. And they exerted antibacterial (Wang et al., 2017), anti-neuroinflammatory (Lin et al., 2016), antimicrobial (Yang et al., 2012), cytotoxic (Wang et al., 2013), antiallergic activities and so on (Morikawa et al., 2006; Morikawa et al., 2006), according to the references. However, their cytoprotective effects on nm SiO_2-induced A549 cells damage were firstly reported. Among them, compounds **3**, **4**, and **8** were certified to increase the cell viabilities and demonstrated to potent ingredients for the development of lung protective reagents. ROS assays results further proved that protective activity may be related to the anti-oxidation.

Another class of compounds reported from plants were phenylethanoid glycosides (compounds **9**–**14**). These compounds possessed anti-neuroinflammatory (Lin et al., 2016; Zhang et al., 2018) and antioxidant activities (Tai et al., 2014). Few studies were performed for their protective effects. Compounds **11**, **12**, and **13** displayed potent protective activities and decreased ROS production significantly. These components could be easily isolated and synthesized to enrich. Therefore, the above two classes of compounds could be served as lung protective candidates due to their low cytotoxicity activities. Further investigations of action mechanisms were explored by compound **8**.

Militarine (compound **8)** inhibited the increase of ROS levels induced by nm SiO_2 and up-regulated the levels of Nrf2 and its downstream target genes, such as *HO-1* and *γ-GCSc*. We also find that militarine reduced the apoptosis rates of A549 cell, reversed the decline of cell activities and the expressions of apoptosis-related proteins. Previous study indicated that direct supplementation of antioxidants to remove excess free radicals could affect the important function of free radicals as information molecules. In addition, direct supplement of antioxidants which are consumed would lose its effect. Therefore, it becomes more important to explore whether militarine is involved in initiating endogenous protective mechanisms to mitigate lung injury caused by nm SiO_2. Nrf2 signaling pathway is the main endogenous signaling pathway to resist oxidative stress and clear ROS. Nrf2 is found to protect TiO2-induced pneumonia and oxidative stress (Delgado-Buenrostro et al., 2014). On basis of these results, militarine inhibited oxidative stress partly through Nrf2 activation, and therefore alleviating nm SiO_2-induced apoptosis of lung epithelial cells.

Currently, many natural source compounds play important role in the prevention of lung cancer through the Nrf2 pathway.

5. Conclusion

In conclusion, this paper firstly reported the protective effects of lung damages of edible herbal *B. striata*. The lung protective effects of BEB were studied *in vitro*. BEB alleviated nm SiO_2-induced cells and lung protective efficacies of compounds were further evaluated by means of SiO_2 nanoparticles-induced A549 cells damages model for the first time. Generation of ROS linked to increased oxidative stress causes oxidative damage and the pathogenesis of several diseases. Stimulation of cells with SiO_2 resulted in a sharp rise in the concentration of intracellular ROS. Compounds **3**, **4**, **8**, **11**, **12**, **13**, **23**, and **25** decreased the production of ROS. These results indicated that these isolates performed protective effects by the reduction of ROS.

Among them, militarine (**8**) could effectively alleviate the lung injury caused by nm SiO_2 suspension *in vitro*. These data indicated that is capable of inhibiting nm SiO_2-induced pulmonary inflammation and oxidative injury in mice.

Authors' contributions

DZ, CWH, and JXQ performed the experiments and analyzed the data; NL, GC designed the experiments; DZ and NL wrote the text. All authors have read and approved the final version of this manuscript.

Declaration of Competing Interest

The authors declare that they have no known competing financial interests or personal relationships that could have appeared to influence the work reported in this paper.

Acknowledgments

This work was financially supported by National Natural Science Foundation of China, China (Grant No. 81872768, 81673323, 82003630), Scientific Research Fund of Liaoning Province Education Department, Liaoning (LJKZ0949), Special Fund of Research Institute of Drug Regulatory Science Research Shenyang Pharmaceutical University, Liaoning (2021jgkx010), State Key Laboratory for Chemistry and Molecular Engineering of Medicinal Resources (Guangxi Normal University), Guangxi (CMEMR2022-B04).

Appendix A. Supplementary data

Supplementary data to this article can be found online at https://doi.org/10.1016/j.chmed.2022.11.001.

References

Bae, J. Y., Lee, J. W., Jin, Q., Jang, H., Lee, D., Kim, Y., ... Hwang, B. Y. (2016). Chemical constituents isolated from *Bletilla striata* and their inhibitory effects on nitric oxide production in RAW 264.7 cells. *Chemistry & Biodiversity, 14*(2), 1–5.

Bai, X., Liu, Y., Wang, S. Q., Liu, C., Liu, F., Su, G. X., ... Yan, B. (2018). Ultrafine particle libraries for exploring mechanisms of PM 2.5-induced toxicity in human cells. *Ecotoxicology and Environmental Safety, 157*, 380–387.

Bolhassani, A. (2015). Cancer chemoprevention by natural carotenoids as an efficient strategy. *Anti-Cancer Agents in Medicinal Chemistry, 15*(8), 1026–1031.

Cai, X. F., Lee, I. S., Dat, N. T., Shen, G. H., Kang, J. S., Kim, D. H., & Kim, Y. H. (2004). Inhibitory lignans against NFAT transcription factor from *Acanthopanax koreanum*. *Archives of Pharmacal Research, 27*(7), 738–741.

Cao, C., Jiang, W. J., Wang, B. Y., Fang, J. H., Lang, J. D., Tian, G., ... Zhu, T. F. (2014). Inhalable microorganisms in Beijing's PM2.5 and PM10 pollutants during a severe smog event. *Environmental Science & Technology, 48*(3), 1499–1507.

Chen, B., Liu, Y., Liu, H. W., Wang, N. L., Yang, B. F., & Yao, X. S. (2008). Iridoid and aromatic glycosides from *Scrophularia ningpoensis* Hemsl. and their inhibition of $[C^{a2+}]_i$ increase induced by KCl. *Chemical Biodiversity, 5*(9), 1723–1735.

Delgado-Buenrostro, N. L., Medina-Reyes, E. I., Lastres-Becker, I., Freyre-Fonseca, V., Ji, Z. X., Hernandez-Pando, R., ... Chirino, Y. I. (2014). Nrf2 protects the lung against inflammation induced by titanium dioxide nanoparticles: A positive regulator role of Nrf2 on cytokine release. *Environmental Toxicology, 30*(7), 782–792.

Duan, X. H., Li, Z. L., Yang, D. S., Zhang, F. L., Lin, Q., & Dai, R. (2013). Study on the chemical constituents of *Gastrodia elata*. *Journal of Chinese Medical Material, 36*(10), 1608–1611.

Feng, W. S., Li, K. K., & Zheng, X. K. (2009). Study on chemical constituents of *Forsythia suspensa* (Thunb.) Vahl. *Chinese Pharmaceutical Journal, 44*(7), 490–492.

Gouvêa, D. P., Berwaldt, G. A., Neuenfeldt, P. D., Nunes, R. J., Almeida, W. P., & Cunico, W. (2016). Synthesis of novel 2-aryl-3-(2-morpholinoethyl)-1,3-thiazinan-4-ones via ultrasound irradiation. *Journal of the Brazilian Chemical Society, 27*(6), 1109–1115.

Guan, H. J., Zhang, X., Tu, F. J., & Yao, X. S. (2009). Chemical constituents of *Dendrobium candidum*. *Chinese Herbal Medicines, 40*(12), 1873–1876.

Han, S. W., Wang, C., Cui, B. S., & Li, S. (2015). Studies on glucosyloxybenzyl 2-isobutylmalates of *Pleione bulbocodioides*. *China Journal Chinese Material Medicines, 40*(5), 908–914.

He, X. R., Wang, X. X., Fang, J. C., Zhao, Z. F., Huang, L. H., Guo, H., & Zheng, X. H. (2017). *Bletilla striata*: Medicinal uses, phytochemistry and pharmacological activities. *Journal of Ethnopharmacology, 195*, 20–38.

Huang, S. Y., Shi, J. G., Yang, Y. C., & Hu, S. L. (2002). Studies on the chemical constituents of *Coeloglossum viride* (L.) Hartm. var. *bracteatum* (Willd.) Richter. *Acta Pharmaceutica Sinica, 37*(3), 199–203.

Jiang, H., Yang, L., Xing, X. D., Zhang, Y. Y., Yan, M. L., Yang, B. Y., ... Kuang, H. X. (2017). Chemical constituents from fruits of *Xanthium sibiricum*. *Chinese Tradition Herbals Drugs, 48*(1), 47–51.

Li, H. Y., Zheng, P., & Xie, X. T. (2006). Isolation and identification of two components in the synthetic agent gastrodin. *Chinese Journal of New Drugs, 15*(15), 1278–1281.

Lin, C. W., Hwang, T. L., Chen, F. A., Huang, C. H., Hung, H. Y., & Wu, T. S. (2016). Chemical constituents of the rhizomes of *Bletilla formosana* and their potential anti-inflammatory activity. *Journal of Natural Products, 79*(8), 1911–1921.

Miao, Q., Bao, H. Y., Piao, S. J., Lin, H. W., & Qiu, F. (2008). Study on chemical constituents of *Duchesnea indica* Andr. Focke. *Acadamy Journal of Second Military Medical University, 29*(11), 1366–1370.

Morikawa, T., Xie, H. H., Matsuda, H., & Yoshikawa, M. (2006). Glucosyloxybenzyl 2-isobutylmalates from the tubers of *Gymnadenia conopsea*. *Journal of Natural Products, 69*(6), 881–886.

Morikawa, T., Xie, H. H., Matsuda, H., Wang, T., & Yoshikawa, M. (2006). Bioactive constituents from Chinese natural medicines. XVII. constituents with radical scavenging effect and new glucosyloxybenzyl 2-isobutylmalates from *Gymnadenia conopsea*. *Chemical & Pharmaceutical Bulletin, 54*(4), 506–513.

Mucha, M., Podkalicka, P., Mikulski, M., Barwacz, S., Andrysiak, K., Biela, A., ... Loboda, A. (2019). Development and characterization of a new inhibitor of heme oxygenase activity for cancer treatment. *Archives of Biochemistry and Biophysics, 671*, 130–142.

Ouyang, W., Gao, B., Cheng, H., Hao, Z., & Wu, N. (2018). Exposure inequality assessment for PM2.5 and the potential association with environmental health in Beijing. *Science of the Total Environment, 635*, 769–778.

Pcolinski, M. J., O'Mathúna, D. P., & Doskotch, R. W. (1995). Modified labdane diterpenes from *Amphiachyris amoena*. *Journal of Natural Products, 58*(2), 209–216.

Song, Y., Zeng, R., Hu, L. L., Maffucci, K. G., Ren, X. D., & Qu, Y. (2017). *In vivo* wound healing and *in vitro* antioxidant activities of *Bletilla striata* phenolic extracts. *Biomedicine & Pharmacotherapy, 93*, 451–461.

Tai, Z., Chen, A., Qin, B., Cai, L., & Xu, Y. (2014). Chemical constituents and antioxidant activity of the *Musa basjoo* flower. *European Food Research and Technology, 239*(3), 501–508.

Tang, Y. P., Yu, B., Hu, J., Wu, T., & Hui, Y. Z. (2001). Chemical constituents from the Bulbs of *Ornithogalum caudatum*. *Journal of Chinese Pharmaceutical Sciences, 10*(4), 169–171.

Wang, L. N., He, Y. Z., Zhao, Q. D., Deng, Y. R., Wu, P. Q., & Zhang, Y. J. (2017). Phenolic compounds from *Bletilla striata*. *Journal of Asian Natural Products Research, 19*(10), 981–986.

Wang, Y. N., Lin, S., Chen, M. H., Jiang, B. Y., Guo, Q. L., Zhu, C. G., ... Shi, J. G. (2012). Chemical constituents from aqueous extract of *Gastrodia elata*. *China Journal of Chinese Material Medicines, 37*(12), 1775–1781.

Wang, Y., Guan, S. H., Feng, R. H., Zhang, J. X., Li, Q., Chen, X. H., ... Guo, D. A. (2013). Elution-extrusion counter-current chromatography separation of two new benzyl ester glucosides and three other high-polarity compounds from the tubers of *Pleione bulbocodioides*. *Phytochemical Analysis, 24*(6), 671–676.

Wei, W., & Hui, M. (2015). Cytotoxic, anti-inflammatory and hemostatic spirostane-steroidal saponins from the ethanol extract of the roots of *Bletilla striata*. *Fitoterapia, 101*, 12–16.

Xiang, Z., Yan, X. J., Wen, J., & Liu, W. (2017). Chemical constituents of whole plants of *Patrinia villosa* Juss. *Chinese Pharmaceutical Journal, 52*(3), 185–187.

Yang, X. Z., Tang, C. P., Zhao, P., Shu, G. W., & Mei, Z. N. (2012). Antimicrobial constituents from the tubers of *Bletilla ochracea*. *Planta Medica, 78*(6), 606–610.

Yao, W. X., Li, Y., Han, L., Ji, X. M., Pan, H. H., Liu, Y., ... Ni, C. H. (2018). The CDR1as/miR-7/TGFBR2 axis modulates EMT in silica-induced pulmonary fibrosis. *Toxicological Sciences, 166*(2), 465–478.

Ying, L., Jiang, J. H., Yan, Z., & Chen, Y. G. (2009). Chemical constituents of *Dendrobium aurantiacum* var. denneanum. *Chemical Natural Compounds, 45*(4), 525–527.

Yue, Z. G., Zi, J. C., Zhu, C. G., Lin, S., Yang, Y. C., & Shi, J. G. (2010). Chemical constituents of *Gymnadenia conopsea* (L.). *China Journal Tradition Chinese Medicines, 35*(21), 2852–2861.

Zhang, D., Zhang, Y., Liu, G. T., & Zhang, J. J. (2006). Dactylorhin B reduces toxic effects of β-amyloid fragment (25–35) on neuron cells and isolated rat brain mitochondria. *Archives of Pharmacology, 374*(2), 117–125.

Zhang, Y. J., Wang, K., Chen, H. C., He, R. J., Cai, R. L., Li, J., ... Guan, X. L. (2018). Anti-inflammatory lignans and phenylethanoid glycosides from the root of *Isodon ternifolius*, (d. don) kudô. *Phytochemistry, 153*, 36–47.

Zhao, Y., Niu, J. J., Cheng, X. C., Lu, Y. X., Jun, X. F., Zhao, X. R., ... Wu, C. T. (2018). Chemical constituents from *Bletilla striata* and their NO production suppression in RAW 264.7 macrophage cells. *Journal of Asian Natural Products Research, 20*(4), 385–390.

Zhou, X. L., La, Y. X., Wu, N. Z., & Huang, S. (2010). Study on chemical constituents of the flowers of *Rhododendron anthopogon*. *Western China Journal Pharmaceutical Science, 25*(2), 132–134.

Zidorn, C., Ellmerermüller, E. P., & Stuppner, H. (2001). A germacranolide and three hydroxybenzyl alcohol derivatives from *Hieracium murorum* and *Crepis bocconi*. *Phytochemical Analysis, 12*(4), 281–285.